Available Online at www.ijcsmc.com/journal
International Journal of Computer Science and Mobile Computing
A Monthly Journal of Computer Science and Information Technology, ISSN 2320–088X, IMPACT FACTOR: 7.056
IJCSMC, Vol. 11, Issue. 3, March 2022, pg.56 – 77

Effective of Modern Techniques on Content-Based Medical Image Retrieval: A Survey

Metwally Rashad[1]; Sameer Nooh[2]; Ibrahem Afifi[3]; Mohamed Abdelfatah[4]
[1]Department of Computer Science & Benha University, Egypt
[2]Department of Computer Science & Tabuk University, Saudi Arabia
[3]Department of Information Systems & Benha University, Egypt
[4]Department of Information Systems & Benha University, Egypt
[1] metwally.rashad@fci.bu.edu.eg; [2] snooh@ut.edu.sa; [3] ibrahim.afify@fci.bu.edu.eg; [4] mohamed.abdo@fci.bu.edu.eg
DOI: https://doi.org/10.47760/ijcsmc.2022.v11i03.008

Abstract— The advancement in medical imaging has resulted in a rapid and large increase in medical images inside repositories. These medical images contain very important information that can be used in many things, including diagnosing diseases. This implies that a precise, efficient way of indexing and retrieving biomedical images is necessary to obtain medical images from such repositories in real-time. CBMIR, therefore, played an important part, where the CBMIR's area is very important in the field of image processing and involves low-level feature extraction and similarity measures for the comparison of medical images such as color histograms, edges, texture, shape. The majority of the methods already in use in CBMIR enhance the retrieval of a medical image and diseases diagnosis by reducing the issue of the semantic gap between low visual and high semantic levels. Also, secure access to the medical image of diverse cases, which are often kept on a network and are susceptible to malicious attacks is considered an important target for all medical practitioners. So, most CBMIRs try to cover this target for the purpose of privacy preservation. So, in this survey, the most advanced (CBMIR) frameworks that were used to reduce the issue of semantic gaps, high dimensionality feature maps were covered, disease diagnosis, and medical image security. Furthermore, the different publicly and standard databases used in measuring the performance of these frameworks also were covered.

Keywords— Medical image retrieval, Medical image security, Semantic gap, Privacy preserving, Image processing

I. INTRODUCTION

The fast rise of digital, multimedia, and storage systems in recent years has resulted in massive image and multimedia warehouses. The advances in digital storage and information delivery benefit clinical and diagnostic studies. Diagnostic and investigative imaging systems in hospitals produce an immense amount of images, contributing to the growth of medical image archives. The implementation of an efficient framework for medical imaging is therefore important to help clinicians access such large databases. Many of the algorithms for the automated analysis of medical images were proposed in the literature to promote the creation and management of these vast databases of medical images [1]–[5]. Also, an effective means of supplementing diagnostics and treatment of different diseases and an efficient tool for the management [6] for managing vast volumes of data may be provided by using the CBMIR. Without these technologies, accessing, managing, and extracting data from such massive

collections is extremely difficult. Also, the retrieval of medical images based on textual details like tags and manual annotations is poor in productivity since they require manpower, clinical skills, and time. Medical image retrieval systems, which can retrieve and identify the images automatically based on the features coming from the images themselves, are so critical. It complements the clinical decision support systems, studies, research, and clinical testing for the purpose of searching in large repositories for relevant information.

CBIR is an image search technology that aims to find images most comparable to a certain query, where the search for images is based on their features, whether low levels, such as color, texture, and shape, or high level. CBIR's success depends mainly on the selected features [7] where the images are represented as features with a high dimension. The similarity between the query and the stored images in the databases is measured using distance metrics such as Euclidean Distance (ED). The encoding of images in terms of features, and the selection of an algorithm for the measuring of similarity, are thus the most significant components of CBIR systems. Although several researchers have researched these subjects widely [8], the most difficult problem in CBIR systems remains that of reducing the problem of the semantic gap. This gap occurs between both the visual input of the human visual system (HVS) and the system of imaging when lost the information in the process of representation of the image from high-level semantic to features of low-level [9] This gap will be reduced by either incorporating domain-specific knowledge or employing machine learning techniques to develop intelligent systems capable of acting like HVS.

Machine learning technology has evolved dramatically, and deep learning systems have been a breakthrough, where deep learning includes numerous algorithms of machine learning for modeling abstractions of high-level data [10] by employing a deep structure that contains multiple nonlinear transformations. Deep learning is modeled after the human brain [8], which its architecture is complex and processes information through transformation composed of multiple layers. Thus, deep learning led to learning the complex features from raw images by a machine (deep networks) without using handcrafted features, this enables us to automatically get feature representations through using several abstract levels to automatically learn features by exploring deep structures. In recent studies, it has already been documented that several fields such as image and video classification [11]–[13], visual tracking [14], speech recognition [15], and the processing of natural languages that effectively implemented using deep learning systems [16].

A. An Overview of Content-Based Image Retrieval

Usually, any CBIR system consists of two stages, one online and the other offline, as shown in Fig. 1 where there is a dotted line separating these two stages. In offline stage was indicated by a dotted line in the figure, where features are extracted from all images inside the databases. These features are also indexed for use in searching after that. In online stage was indicated by a solid line in the figure, where the same process of extracting features is carried out on the query image that was executed on the images in the offline stage, and then we use one of the algorithms that measure the similarity to calculate it between the query and the indexed features. After that, the most similar images are retrieved based on their arrangement, from the closest to the lowest according to the measurement.

Different descriptors at a global level have been created over the last few decades to represent images, for example in features of shape, color [17], and texture-based feature [18]. Eakins [19] divides the features of the image into three levels. The spatial location to elements of the image and colors are considered from the features of level one in addition to texture and shape. The features that are derived or logical features are considered from level two, which implies a degree of inference with regard to the identities of the objects in the image. The features into the final level are considered recognized as abstract attributes, and they involve complex inference about the significance of objects belonging to the image. Shape and color are considered significant features in images, where various visual indications are given by the shape, such as characteristics of curve, contour, and surface, while powerful visual cues are provided by color dominate color imaging. The features of texture spatially organized the pixels in an image. These features need standard tools to analyze like Gabor filters [19], Fourier transforms, and wavelets. In addition, there are some local descriptors that have been developed like Scale Invariant Feature Transform (SIFT) [20], Speed Up Robust Features (SURF) [21], and model of Bag of Words (BoW) [22]–[24]. The semantic gap problem was tried to address in various studies [25]–[27], but the features used in these studies cannot fully able address this problem. The SIFT features are used in [25] as a representation of images of the training and query and the performance of the system was tested by using two classifiers, where the classification and indexing

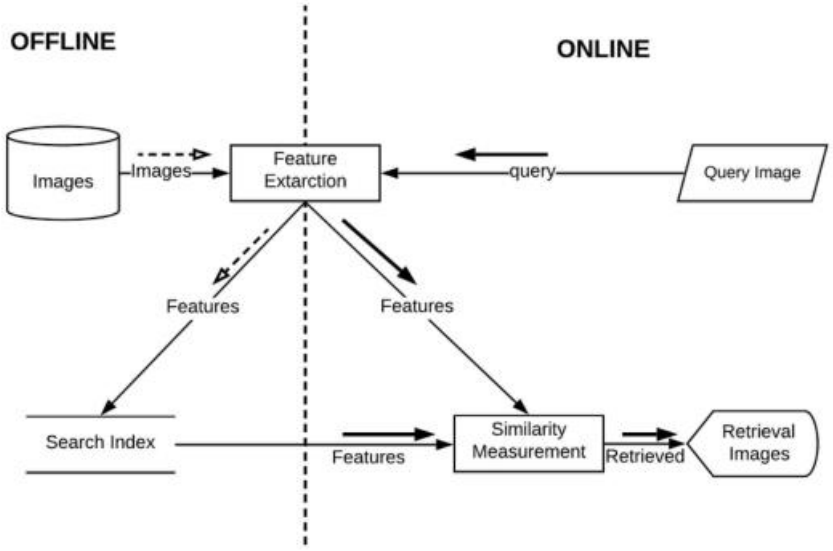

Fig. 1: A generic CBIR architecture.

done by algorithms of the nearest neighbor and KD tree with the best bin first (BBF). A modified voting approach called nearest neighbor distance ration scoring (NNDRS) is developed, where the scores of candidate images are aggregated and the aggregate scores are then sorted into descending order, after that the images with top rank are retrieved. In [26], a general image CBIR system is introduced with Three features for representing the images in the space of feature. Color and texture features are considered low-level, while the structure of the binary tree is utilized to capture higher levels. HSV is utilized for the features of color, while wavelet decomposition is employed for features of the texture.

II. **DATASETS**

In this section, we introduce the various medical image databases that are used in most medical image retrieval.

A. MESSIDOR Dataset

The MESSIDOR dataset [28], illustrated in Fig. 2, contains 1200 eye fundus numerical images on Topcon TRC NW6 non-mydriatic returninograph with 45-degree eld of view taken by 3 ophthalmologic departments utilizing a color video 3CCD camera. The images were taken with 8 bits per color plane at 1440×960, 2240×1488, and 2304×1536 pixels. The number of images for pupil dilatation that was collected was 400 images and without dilatation 800 images. The 1200 images are packed in three sets, one each department of ophthalmology. Each collection consists of 4 zip sub-sets, each of which has 100 TIFF images and an Excel spreadsheet, each providing medical diagnoses of the images.

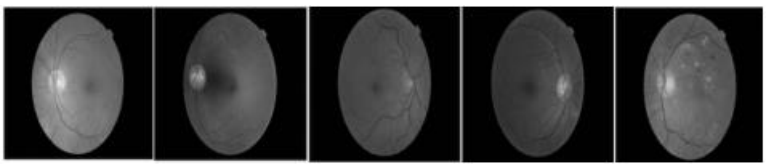

Fig. 2: Sample images from MESSIDOR dataset.

B. Multimodal Dataset

Multimodal dataset including diagnostic images in different modes (MR, PET, OPT, CT, PT, X-ray, etc.). This dataset was divided into 24 classes based on body organ, e.g. lungs, brain, liver, etc, where 22 classes contain cancer images, and the other 2 classes include MESSIDOR dataset [28] and a knee image open-access website [29]. The number of images in the Multimodal dataset is 7200, as there are 300 images in each class. Fig. 3 shows sample images from the Multimodal dataset.

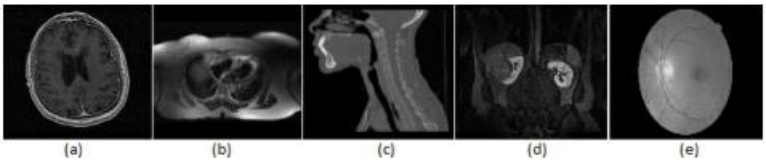

Fig. 3: Multimodal dataset consisting of different body part (a) Brain (b) Liver (c) Thyroid (d) Kidney (e) Eye.

C. Kvasir Dataset

Kvasir dataset [30] as shown in Fig. 4 consists of 4000 images that qualified endoscopists have annotated and confirmed. Based upon endoscopic, pathologic, or anatomical identification, these images were classified into 8 different classes. The range of dimensions for each image is from 720×576 to 1920×1072 pixels. There are 500 images per class.

Fig. 4: Kvasir dataset consisting of endoscopic images (a) Polyp (b) Z-line (c) Dyed-resection-margins (d) Normal Pylorus (e) Cecum .

D. IRMA Dataset

IRMA dataset [6] consists of scanned grayscale X-ray images of the different parts of the body in various modalities and orientations that are distinguished by contrast and intensity variation. Fig. 5 shows an example of images from the IRMA dataset.

Fig. 5: Example images from IRMA dataset.

E. Emphysema-CT Image Dataset

The dataset [31] composed of 115 high-resolution CT (HRCT) slices and 168 manually annotated square patches in a sub-set of the slices. There are 168 61×61 pixel patches from three diverse types of emphysema-CT patches as shown in Figure 6, PSE (59 observations), CLE (50 observations), and NT (59 observations). The NT patches were annotated in never smokers, CLE and PSE ROIs healthy smokers and smokers with COPD in areas of the leading pattern. Regarding the slice, there are four separate types of emphysema-CT slices, PSE, CLE, NT, and pan lobular emphysema (PLE). Fig. 7 shows sample images from the Emphysema CT slices.

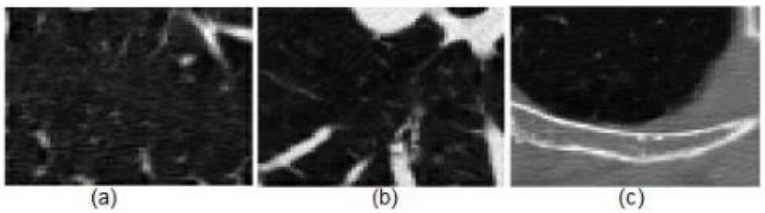

Fig. 6: Emphysema CT Patches images. (a) NT, (b) CLE, (c) PSE

F. NEMA-CT Image Dataset

The NEMA-CT image dataset [32] is consists of the National Association of Electric Manufacturers (NEMA) images in DICOM format and these images are CT that represent various body parts and their process of morphological modification over time. Fig. 8 shows some images from the NEMA-CT dataset.

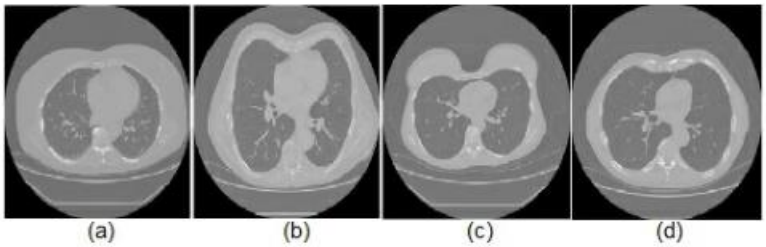

Fig. 7: Emphysema CT Slices images. (a) NT, (b) CLE, (c) PSE, (d) PLE

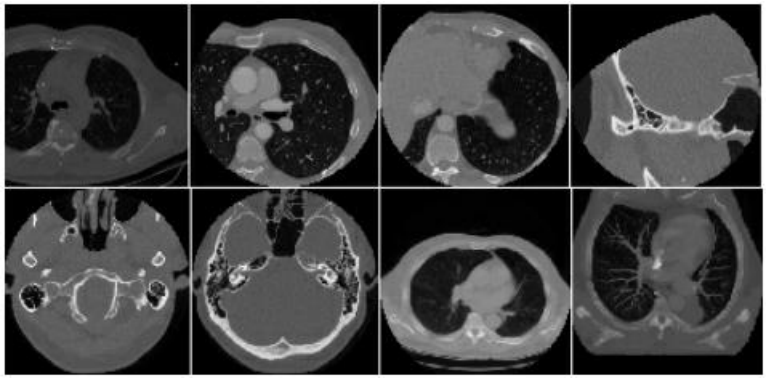

Fig. 8: Some images from NEMA-CT dataset.

G. TCIA-CT Image Dataset

The cancer image archive (TCIA), which was compiled by the authors in [33] and contains a huge number of cancer images [34]. This database contains 604 CT images in DICOM format with series number 1.3.6.1.4.1.9328.50.4.2 of study instance UID 1.3.6.1.4.1.9328.50.4.1 for subject 1.3.6.1.4.1.9328.50.4.0001. The TCIA-CT collection is divided into eight classes, each of which contains 75, 50, 58, 140, 70, 92, 78, and 41 images. The TCIA-CT dataset samples for each class can be viewed from Fig. 9.

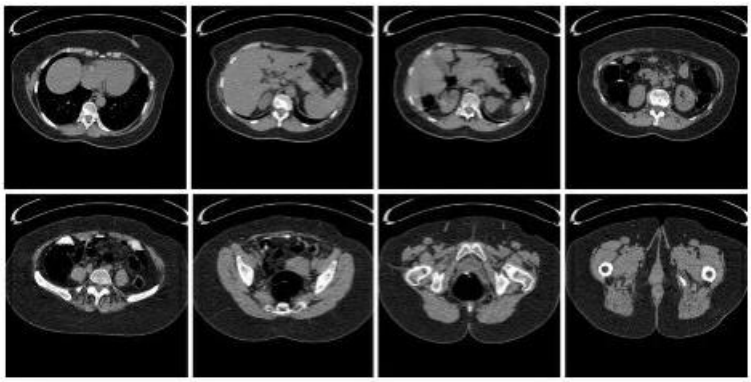

Fig. 9: Sample images from each class of TCIA-CT dataset.

H. NEMA-MR Image Dataset

The NEMA-MR image dataset was created and formed with the image format DICOM from the National Association of Electric Manufacturers (NEMA) [35]. NEMA-MR comprises several MR images that represent various body parts and their process of morphological modification over time. Fig. 10 shows sample images from the NEMA-MR dataset.

Fig. 10: Sample images from NEMA MR dataset.

I. OASIS-MRI Image Dataset

OASIS-MRI [36] illustrate in Fig. 11 is a type of bio-medical dataset created by the Image Studies Open Access Series (OASIS) with MRI. Within the original datasets, a sectional range of 416 topics between 18 and 96 years can be studied and analyzed. These images are difficult to recognize and get from a specific query image. Since it is difficult to evaluate each image's label closely with our eyes, it will be harder to test it with a computer.

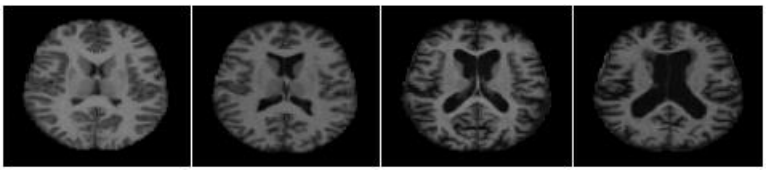

Fig. 11: Sample images from OASIS-MRI dataset.

J. KIMIA Path960 dataset

The KIMIA Path960 dataset [37] comprises 20 histopathological image classes created by the epithelial, muscle, and connective tissue set, where each class contains 48 images. Besides, the images of each class have certain characteristics in which there are high differences in intra classes and certain similarities between different classes. Fig. 12 shows sample images from the KIMIA Path960 dataset.

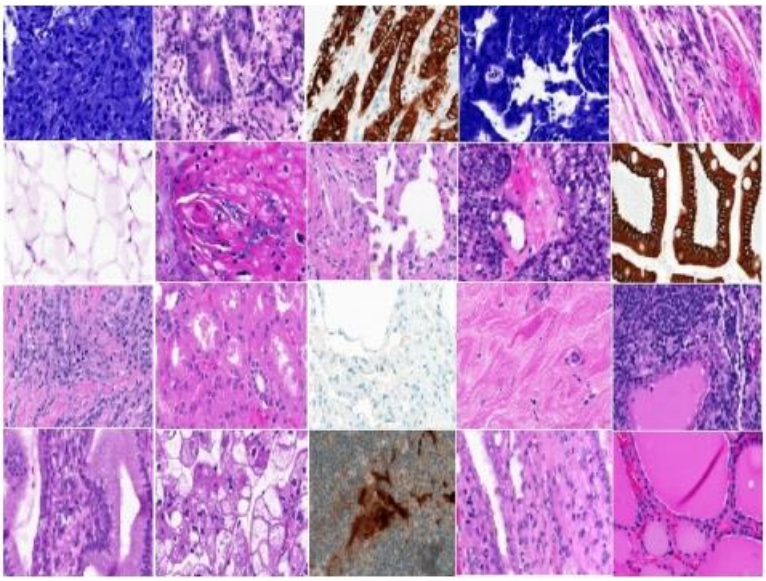

Fig. 12: Sample images from KIMIA Path960 dataset.

K. VIA/I-ELCAP Dataset

VIA/I-ELCAP dataset [38] offers a collection of CT images to compare different diagnostic systems with computer assistance. There are currently 50 low-dose recorded whole-lung CT scans available in the dataset for detection. In a single breath-hold, the slice of CT scans was gathered with the thickness of 1,25 mm. The nodules locations detected by the radiologist are also indicated. Fig. 13 shows sample images from the VIA/IELCAP dataset.

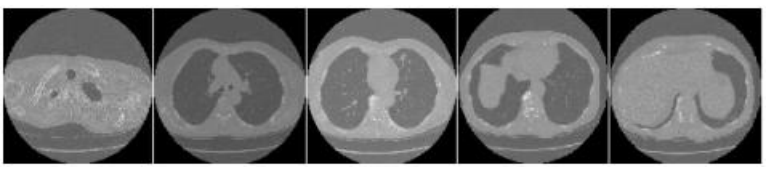

Fig. 13: Sample images from the VIA/I-ELCAP dataset.

L. Extraction of Airways from CT 2009 (EXACT09)

EXACT09 is a chest CT scanning database [39]. This archive contains images from two collections of training and testing, each containing 20 cases. For the saving of CT Scan Image, the DICOM format is used. Fig. 14 shows sample images from EXACT09-CT.

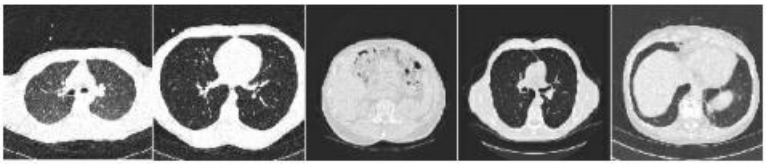

Fig. 14: Sample images from EXACT09-CT dataset.

M. BreakHis Dataset

The dataset [40] is captured from 82 patients with breast tumors. Involve 7909 hematoxylins and eosin (H& E) stained microscopy images. The dataset is composed of four magnification levels of images 40×, 100×, 200× and 400× with the resolution of 700×460 and each image in the dataset is labeled with two main-classes involving benign and malignant as well as eight sub-classes involving four histological distinct types of benign breast tumors: adenosis (A), phyllodes tumor (PT), fibroadenoma (F), and tubular adenoma (TA); and four malignant tumors (breast cancer): mucinous carcinoma (MC), lobular carcinoma (LC), ductal carcinoma (DC), and papillary carcinoma (PC). Fig. 15 present sample images from BreakHis Dataset.

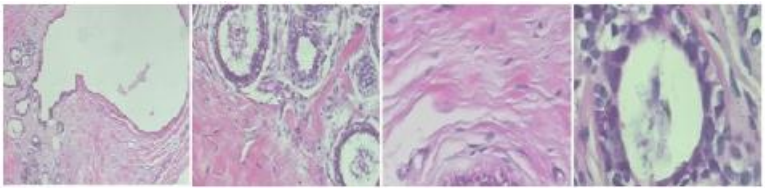

Fig. 15: Sample of breast histopathological images with different levels of magnification.

N. PLOSONE Dataset

The dataset [41] is composed of 285 H& E microscopy images captured at 200× magnification with the resolution of 2048×1536, and the dataset is labeled with four classes involving normal tissue, in situ carcinoma, benign lesion, and invasive carcinoma.

O. MAMMOSET Database

MAMMOSET [42] consists of three different sources of mammograms (DDSM, MINI-MIAS, and VIENNA) in regions of interest (ROIs). On this basis, MAMMOSET images were acquired and annotated in a distinct manner from different medical scanners. This can be used in multiple supervised and non-supervised functions, such as classifying, data visualization, clustering, and CBMIR.

P. ILD database

An incorporated resource for images of interstitial pulmonary illness and clinical data in the ILD database [43]. The database is primarily aimed at providing radiological and clinical data information for ILD patients for research and study purposes. The sample consists of 130 patients with pulmonary CT scans. Every ILD scan is labeled to emphasize the disease region by proficient radiologists.

Q. Brain-Tumor Datbase

The brain tumor dataset [44] consists of 3064 CE-MRI weighted images of 3064 T1, collected from about 233 patients, contrast-enhanced. The dataset consists of 708 portions of meningioma tumor, 1426 portions of glioma tumor, and 930 portions of pituitary tumors. Sample images for each group are shown in Fig. 16. Note that the Brain-Tumor database is a large-scale database.

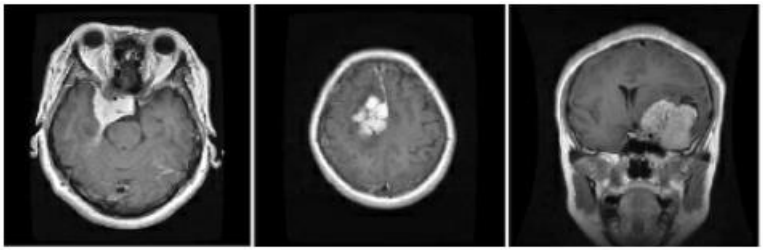

Fig. 16: Sample images for each tumor category from the dataset.

R. Lung Image Database Consortium and Image Database Resource Initiative (LIDC-IDRI)

The LIDC-IDRI [45] is a publicly accessible dataset of lung images comprising 1,018 medical research cases, each with CT images and XML files with annotations. The dataset comprises a total of 244,527 CT slices with a size of 512×512 pixels. Some original CT images are provided in Fig. 17. Further, a total of 36,378 nodules, including 11,509 nodules with diameter < 3 mm and 19,004 non-nodule, were labeled. Four authoritative radiologists independently labeled the pulmonary nodules in LIDC-IDRI in two stages, which are further split into six categories.

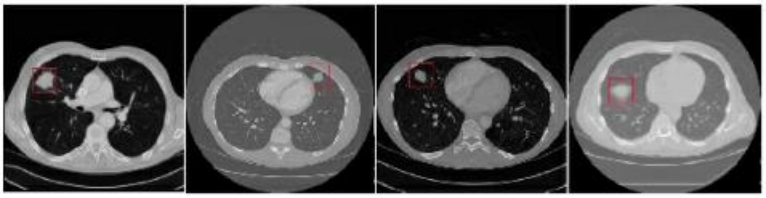

Fig. 17: Examples of CT image on lung cancer in the dataset.

III. MODERN METHODS APPLIED ON MENTIONED DATASET

In this section, we introduce and summarize how modern methods applied to the mentioned dataset work, mentioning the advantages and disadvantages of each method. Also, we show in Table I the summarization of mentioned methods in terms of the model, the dataset used by each method, classification technique applied to the dataset, feature vector length, extraction and retrieval time, and the accuracy of the model for each dataset.

In order to enhance the process of identifying dominant features, researchers aim to provide the best models and descriptors to increase the quality of medical image retrieval. In [46] a new CT image retrieval image descriptor was suggested for a local wavelet (LWP) pattern. Firstly, the decomposition of the local wavelet takes place in the local pixel area to encode the relationship with the neighboring pixel. Secondly, the local wavelet was compared to the center pixel transformed values for the encoding relationship between the center and neighboring pixels and calculate the LWP pattern for the center pixel. Thirdly, they generated the LWP for every pixel of the image and eventually used it as a feature vector to find the histogram. The LWP feature descriptor was tested using three CT medical image retrieval studies on three medical CT-image bases (NEMA-CT database, EXACT09-CT database, TCIA-CT databases), and compared LWP with LTP descriptors [47], LTCoP [48], LBP [49], and LMeP [48]. From the experiments, the LWP feature descriptor executes the current feature descriptors for each database, where the LWP is superior to almost every group within each database, and the LWP feature descriptor's time complexity decreases. The local neighbors that influence the LWP dimension are only taken into consideration as a local neighbor. Experiments and research show that their LWP feature descriptor can be used more easily, reliably for the medical CT image diagnosis, but the high-level semantic information is not fully extracted from the image.

Hand-crafted features can negatively influence medical image retrieval. So, we have found in [50] unique feature for medical imaging, where a histogram of compressed scattering coefficients was suggested (HCSCs). Their method works as follows: Firstly, invariant representations of its translation A scattering transformation to a medical image was carried out. Secondly, they employed the BoW-frame to drive the histogram as a feature vector after the compression process. Thirdly, to assess the features efficiency of the HSCSs, their method was applied using three CT image databases, namely NEMA-CT, EXACT09-CT, and TCIA-CT respectively. The result of the experiments proved that their method has been achieved high performance compared to many features, such as LWP, LMeP, SS-3D-LTP [51], and LBP. Despite these advantages, but it has some drawbacks. Firstly, the HCSC

used partial image information as it allows only one path of projection for compression. Secondly, the time consumption arising from the derivation of the codebook used in the BoW model due to the clustering process that affected the efficiency of the HCSC adversely.

A simple method to use the texture features for retrieval of the medical images has been suggested in [52]. This method is considered more efficient and discriminative compared to recent methods such as HCSCs [50], where just 21% of the time spent in HCSC scattering transform for the image filtering and partitioning operation. The images in this method are filtered with different filters from Gabor and Schmid and the filtered images are then divided into patches that do not overlap. Finally, they used the BoW model to represent the features of images. This method applied to two benchmarks CT databases EXACT09-CT, and TCIA-CT, where the experiments showed their superiority compared to the recent methods. However, somewhat it did not reduce the semantic gap significantly too.

Due to the restrictions in [50] which influence the results' accuracy. A novel and integrated scattering feature for the retrieval of medical images was thus proposed in [53]. The method proposed combines two types of compressed dissemination data from a variety of points of view, namely data concentration (DC) and canonical correlation analysis (CCP), where the feature presented takes account of the relevant scattering data capable of high-level representations of the original medical image. For the validation of the method, two of the CT image databases, EXACT09-CT, and TCIA-CT, have been used in their process. The experiment results demonstrated high performance compared to other current featured methods including LWP, HSCSs, LMeP, SS-3D-LTP, and LBP. Their system has proven high performance. Given these benefits, it has also some disadvantages because the application of the scattering transformation is often time-consuming.

A new descriptor has been proposed in [46] for biomedical images retrieval and indexing called local bit plane decoding pattern (LBDP), where for LBDP binary pattern creation, in each plane the LBDP transforms the local district, encoding the relationship between the center pixel intensity value and the values that are transformed. The structure of the LBDP process differs from the existing descriptors of the features belonging to the image. In their approach, the dimension was depending on the image bit depth and local neighbors count. So, three tests of the retrieval for the biomedical images were carried out to assess the improvements and efficiency of LBDP discriminating in terms of ARP, ARR, and F_{score}. Two databases of CT images (Emphysema-CT, and NEMA-CT) and one MR (OASIS-MR) repositories are tested to prove that LBDP is above these current modern descriptors. The time to retrieval with LBDP is considerably reduced while simultaneously increasing efficiency. Furthermore, the outline of the LBDP feature may also be employed in an invariant face recognition task. But, this approach includes a disadvantage where the system has relatively low output because the high level of semantical information is usually not defined as within the mind of the user. In [54] proposed a new extract approach that relies on the extraction using the Gray-level Co-occurrence Matrix (GLCM) [55] and the local pattern descriptors (LPD) of texture features from medical images. To gain improved retrieval output on medical images in order to make quick decisions in clinical applications. The Local Mesh Vector Co-occurrence Pattern Descriptor is presented (LMVCoP). Through integrating the LPD with the GLCM the LMVCoP extracted textural features in the MRI brain images. LMVCoP has been compared to existing descriptors, such as the LTCoP, LMeP, LBDP, PVEP, and LVP [56], for performance appraisal measures. Their outcomes are evaluated in terms of evaluation metric accuracy. The LMVCoP descriptor has been used on the MR (OASIS-MR) database, where 87.57% of ARP was achieved and 53.21% for ARR. The time used for extraction of features of LMVCoP descriptors is 04.29 s and for retrieval is also 0.21 s which is considered less. The results of the simulation and the experiments have shown that the LMVCoP exceeds the other state-of-the-art. Such improvements, however, have a disadvantage, where the dimension of the feature vector is very large, and it is highly inefficient to index and match processes.

A new method characterized by encoding the relationship among neighbors was suggested in [57], where the method takes into account multiple image dimensions, in order to encode information on the local depth. It also searches for directional edges and retrieves local information in many directions. This method was applied to three benchmark databases MESSIDOR (Retinal images), OASIS-MRI, and VIA/I-ELCAP (CT images) respectively. The result of experiments proved the superiority of this method to retrieve images accurately compared to the recent methods, where the other methods considered the one-dimensional images information in most literature for encoding, resulting in less accuracy for retrieval, for example, LMeP encodes the neighboring neighbors' relationship and LBP encodes the neighbor's relationship to the center pixel. Although this superiority, this method has some drawbacks, where it has a high dimensional feature vector that leading to an increase the

computational complexity and failed to not fully extract the high-level semantic information from the image.

In [58] they proposed a method that utilizes two forms of profound neural network techniques: a supervised model of learning for convolutional neural networks, (CNN) and a non-supervised model of training, is stacked with denoising autoencoders (SDAE) to represent the most discriminatory features of medical images. In addition to index all images to look for related images. For the first time, they employed preferential learning technology (PL) to learn and train a model reference image capable of generating a list of the ranked image of similarities from the database of the medical images. They have carried out a great trial of three databases of different complexity levels (NEMA-CT image database, image database OASIS-MR, database TCIA-CT) to investigate whether the method proposed would provide reliable output over medical databases of various formats and types of imagery. The method is compared with the descriptor for the local binary pattern in [49]. The results of the experiments have shown that this method makes all datasets with high accuracy in comparison to other modern technologies and reduces computing complexity by utilizing the preference learning (PL) model as a supervised ranking algorithm. This method also has a disadvantage, where the deep neural networks need to be fine-tuned with large-scale biomedical images acquired to extract more professional features.

One aspect of the success of any (CBMIR) is its ability on the feature extraction that describes the high-level semantics in images. So, in [59] they suggested a novel method for biomedical image retrieval utilizing the Zernike moments (ZMs) [60]. ZMs belong to the global descriptors group and are orthogonal moments. ZMs acquire gross image information that extractors of the local feature like LBP, LDEP [46], and others cannot obtain. This broad perspective is excellent for distinguishing medical images from various regions of the body precisely. Furthermore, their noise insensitivity makes them ideal for the retrieving of images that are real-life, which are commonly harmed by noise. In order to evaluate the method, they have applied their method using two image databases, namely EXACT09-CT, and OASIS-MRI respectively. The experiment showed that when compared to other known features such as LBP, ULBP, or LDEP the methodology of ZMs-based methods has achieved high performance and other states of the art recently released methods like SS-3D-LTP, LBDP, LMePVEP [61] and CSLBCOP [62]. Despite these advantages, it has some drawbacks. Firstly, the outer circle mapping method has been used for computing ZMs. The use of outer circle mapping might result in inaccurate image retrieval. Secondly, the images in the classes of both the Emphysema-CT and OASIS-MRI databases appear to overlap in the existence of noise, i.e. to fall into another class, thereby causing incorrect retrieval. Thirdly, fewer features of the ZMs are used for classification purposes. Finally, in the Emphysema-CT and OASIS-MRI databases, tiny images lead to poorer retrieval levels when they may be connected.

In [63] a new method for the enhancement and resolution of the major problems in [58], [59], and in the majority of modern methods, where orthogonal Fourier-Mellin Moments (OFMMs) was suggested. OFMMs have several features, such as greater information packing power, small feature dimensions, improved image noise robustness, rotation invariance, and scaling, as a result, they are ideal for applications of retrieval biomedical images. When compared to other state-of-the-art methods like (Local Binary Pattern (LBP), Local Ternary Pattern (LTP), Local Quinary Patterns (LQP), etc..)., this approach is also incredibly efficient since it requires very few CPU seconds to obtain the top images that are matched to the query. They have applied their method on four various medical databases namely the Emphysema-CT, NEMA-CT, OASIS-MR, and NEMA-MR. The results show that the rate of retrieval from all current methods for noisy and non-noise images of each of the four medical test bases improved considerably by around 20% and 7% (average) respectively, but this method has disadvantages, where the major difference between multimodal datasets when working with a large dataset may not be very satisfactory.

A robust descriptor for features named the antithetic isomeric cluster pattern (ANTIC) was suggested for CBMIR and modification applications in [64]. The ANTIC is inspired by isomerism, which uses ANTI and clustering characteristics. It is able to extract information about the line and corner points in the local neighborhood and therefore provides a robust texture descriptor. In addition, only four isomeric antithetic patterns are needed for all directional information to be obtained. By reducing the length of the feature vector, this trait ensures robustness. Furthermore, the MANTIC, which combines multi-resolution information using Gaussian filters, also improves its performance. This descriptor has been applied to four benchmark databases MESSIDOR, NEMA-CT, OASIS-MRI, and VIA/I-ELCAP, where the experiments showed their superiority compared to the recent methods. However, it did not reduce the semantic gap somewhat, as well as although the

length of the feature vector was reduced to half, but still large somewhat.

In [65], an effective approach has suggested retrieving biomedical images using the global and local image features. The local binary edge directional pattern (LDEBP) has been developed to extract local features, where information for each pixel in the image is collected from every direction, i.e. 0_0, 45_0, 90_0 and 135_0. Directional information shall be calculated based on the magnitude of the local signals code between the central pixel and its directional pixels. All spatial information is used for the evaluation of four edges for each pixel. Local and shape features of the image have been derived from the Lower Order Zernike Moments (LZMs) [66]. Once the shape and texture descriptors were integrated, the results were improved. Such results also demonstrated substantial progress when applied to benchmark databases such as Emphysema-CT, OASIS-MRI, brain tumor, and compared to validated approaches such as LBDP, ZM, and LDEP. Yet, there is a downside to all these enhancements, where the time for extraction and retrieval is comparatively growing compared to some other approaches.

In [67] a new indexing and retrieval method for medical images was proposed as a kind of improve CBMIR retrieval. The local binary AND pattern threshold (TLBAP), as well as the adjacent local average differential pattern (LANADP), were proposed as two new descriptor features. Every descriptor has been added to medical images, every descriptor generates a histogram and at the end, the two histograms are combined in order to create the last features vector. Various description patterns, such as the local binary pattern (LBP), are considered to be the binary pattern threshold for each pixel center in the image, but the TLBAP descriptor improves LBP uses the highest pixel intensity of neighboring pixels in calculating the threshold value. Then, they perform a logical AND operation between the LBP pattern and TLBP pattern to generate a TLBAP pattern. Furthermore, the other descriptor (LANADP) was suggested as a way to extract all dominant features and reducing the semantic gap by finding the relationship of adjacent pixels to their next neighbors in the diagonal, vertical and horizontal direction. They have used three databases of biomedical images , namely, NEMA-CT, OASIS-MRI, and VIA/ELCAP-CT, for testing the efficacy of their method in comparison with the other methods. All the experiment results of the proposed method were superior. However, all these improvements in retrieval efficiency have a downside, where the retrieval duration is significantly longer than the other methods.

The majority of the conventional methods in (CBMIR) perform fairly poorly because they often do not define the user's high-level semantic data. Finally, the rapid development of deep learning has brought higher performance and versatility than traditional descriptors in standard image retrieval tasks to features obtained from pre-trained CNN models. In [68] a new CBMIR (CNN) and Hash coding framework has been built. The new framework uses a Siamese network that uses image pairs (similar and dissimilar) to generate images of the same class and uses a contrasting loss function and weight sharing to learn how to create images of the same class. The CNN is used to extract features from each of the network branches and reduces via hash-mapping the dimension of the features vectors. During training, a novel loss function has been created, which would make the feature vectors more included and allow real value outputs to approx. the required binary values. The trained network generates the compact binary hash code of the image query and is comparable with the hash code of database images during the retrieval process. Two medical image datasets were used the (VIA/I-ELCAP) and the TCIA-CT [69]. Experimental tests have proven that this method is better than the current solutions to CNN and hash. Also, in comparison with the conventional CNN methods in which the Siamese network is paired with the Hash system, the solution is superior.

In [70] they wanted to handle the limitations of current handcrafted methods of extraction of features. So, a new feature learning method was thus suggested to address these limitations and extract from medical scans the robust features. The proposed feature learning method is separated into two phases: the first is an IR-Net (image reconstruction network), which is meant to reconstruct the supplied input image using a unique deep network encoder-decoder. The suggested IR-Net was utilized as a new encoder network to encode the image to a variety of features and to reconstruct the input image using a new network of decoders. They have shown that the encoded features represent the input image in a strong way if the input image is properly reconstructed. In the second phase, these features that are encoded are used in the retrieval of medical images. In three medical image databases, they assessed the output of the method, namely OASIS-MR, ILD, and VIA/I-ELCAP CT, in comparison with the existing methods the new methodology was exceeded them with the accuracy of the results, but this method has some limitations, where it is not viable for multimodal medical image retrieval because they developed a CBMIR system that retrieves medical images that have a disease close to the input medical image.

A new 3D local-oriented zigzag fused pattern descriptor (3D-LOZFP) was proposed in [71] for the purpose of retrieval of CT images. The three distinct 3D zig-zag patterns in four directions on a 3D plane are used by this descriptor to encode the link between the center and the neighboring pixels. In total, there have been 12 effective 3D zig-zag patterns. The 3D plane is created through a Gaussian filter bank which generates numerous, multi-scale, filtered images. A high dimension vector was produced by this descriptor. The number of features was therefore decreased utilizing a quantization and fusion technique. This method applied to two benchmark CT image datasets the NEMA-CT dataset and the TCIA-CT dataset. The results of the experiments have shown that this method is highly efficient relative to other recent methods. Although this superiority, this method has some drawbacks, where it failed to extract the high-level semantic information from the image and the feature extraction process is considered time-consuming.

A new deep hashing method is suggested in [72], in which the operations of deep extraction, binary code learning, and deep hash function learning are conducted under supervision. The discreet restricted objective function in the learning of the hash code is particularly iteratively optimized so that the binary code may be solved without the requirement for relaxation. Semantic similarity is retained in the meantime by exploring supervision information in discreet optimization in order to apply a principle of graphical regularization to the neighborhood structure of the training data to conserve them. Furthermore, for re-ranking the images a new scheme to refine the measure of similarity by considering the Euclidean Distance among realistic descriptors and their category data between these images is proposed to increase the ranking of the returned medical images with a specific hamming distance. This method was applied to the pulmonary nodule image dataset (LIDC-IDRI), where the experiments show its superiority compared to the recent methods. However, it requires a sufficient amount of excellent quality labeled data, which are not readily available, to create models.

In [73] a great solution was presented to enhance the efficiency of CBMIR with the application of a deep learning system for the purpose of CBMIR by training a deep convolution neural network (DCNN). Introduced two methods for medical image retrieval; one is a class prediction by the trained network to predict the class of the query image and then search for images that are appropriated in that specified class. The second method is to not combine any information on the query image class and check for appropriate images in the entire database. The presented method reduced the semantic gap by learning discriminating features directly from images. The suggested method can achieve a mean average precision of 69% and average classification accuracy of 99.77% in the retrieval task. The most suitable method to obtain a multimodal medical images dataset for various body parts is the method provided, but this method has an adverse effect whereby fully trained DCNN-based methods demand a large collection of labeled medical images to achieve their full potential and the feature dimension is 4096, that is highly time-consuming.

In [74], they suggested a method for solving the CBMIR system problem based on handmade features, i.e. inefficient content modeling, high dimensional features, and extraction of unnecessary and less useful features. An effective method has been used to represent images utilizing outstanding convolutions features. They worked on AlexNet's initial convolutional layer of kernels, demonstrating how visual content may be produced successfully by collecting color and texture features. Two measurements, texture sensitivity, and color sensitivity were used to study the properties of these kernels. On the basis of these discoveries, three different clusters divided the convolutional feature space, where there are a number of kernels with similar features in each of these clusters. These individual kernel sets are utilized to extract texture and color features from the image and to add them to a single feature map termed the Spatial Maximum Activator Map (SMAP). The features of these maps have been recorded in a histogram so that their spatial layout information is also obtained with a structured pooling technique without increasing the dimensions of the features. This allows them to extract various strengths from the features of texture and color while clustering the space for convolution. Furthermore, the spatial maximal activator map (SMAP) approach enables them to choose the most discriminative features. The Kvasir dataset comparison of the classification performance indicates that this method has the best precision of 75.4, also the comparison of the retrieval performance with existing feature extract on methods shows that this method has the best retrieval performance with Average precision retrieval of 74.02 @50 but this method has a drawback, where a huge collection of labeled medical images is required for training to reach its full potential.

In [75] a new method has been introduced to reducing the semantic gap issue and achieve high accuracy in the retrieval of multimodal medical images over existing state-of-the-art methods. The suggested solution was tested with the two standard datasets, namely, the Kvasir dataset, and the

IRMA 2009 dataset. It was an efficient way to pick a perfect subset of features from pre-trained convolutional CNN layers. They found that the chosen subset of features is much better than the entire set of features in large datasets of medical image retrieval. They have also suggested a highly efficient method for depicting such features as compact binary codes using Fast Fourier Transform (FFT) to reduce the search space and enhance medical image retrieval efficiency. The vector of the feature is patronized as a one-dimensional signal and transformed by FFT into the frequency domain. Then, they transformed the feature vector into bits on the basis of their selection, using a simple linear transformation, by selecting the necessary number of frequency components and they used the binary codes obtained to provide hash codes and allow efficient retrieval of big data sets. This proposed hash code method was compared extensively with many state-of-the-art methods, several of which outperformed significantly. However, with very shortcodes, the proposed method was not successful, mainly because the Fourier spectrum was easy to convert to binary codes and also the method did not obtain a high average accuracy at a 50-image accuracy in the Kvasir data set compared with the approach in [74], where that approach reached 47%, but in [74] 74.02%. The performance was in addition low compared to spherical hashing (SpH) [76], sensitive hashing (DSH) [77], and random-rotation principal component analysis (PCA-RR) [78]. However, efficient FFT-based codes computation time makes them more suitable for use.

The researchers have continued to improve the methods proposed in [73], [75] in which a new technique is applied which seeks to reduce semantic gaps and obtain the best possible results, Therefore, in [79] have been proposed new (CBMIR) system that focused on the spatial matching of visual words and a new similarity metric, the "Skip Similarity Index" (SSI), is efficiently utilized in computing visual word similarity spatial similarity. The results of the experiment exposed that it's most successful in extracting multimodal image datasets from various body organs and with similar anatomical structures. The mean Average Precision (mAP) for the retrieval process of 69.70% was achieved in the proposed method. Nevertheless, the method did not achieve a high-precision average retrieval of 50 images on the Kvasir dataset as opposed to the method in [74] where 74.02% had been achieved, but [79] had 60.48%. Even when comparing the images in the whole database to establish similarity, the computational complexity of the suggested technique is substantial when compared to standard BoVW techniques.

More was made at [80], when a modern medical image retrieval technique was introduced more reliable than that used in the previous methods to retrieve images using a topic location feature vector from a huge database of multimodal medical images. In order to obtain a topic probability, the Guided Latent Dirichlet Allocation Model (GuidedLDA) is used and the suggested location model is used to determine the location probability. The location model is depicted in images of each topic as the standard distribution of visual word locations. The location likelihood of the images was evaluated based on the closeness of the location of visual words in the established location models. The feature vector was created by combining the topic and location probability of visual words in the images. The significant position information into the topics has reduced the problem of the semantic gap, where the images were represented by a low-dimensional location feature vector. By predicting an image label using the topic-location feature vector, search times have been decreased by avoiding a full search for images that are similar over the whole database. The location weighted precision (wPrecision) was introduced and became a better way of evaluating the normal precision metric set of medical images. Experiments demonstrate that including spatial information in the topics improved the performance of CBMIR of a medical image when compared to other modern retrieval systems of medical images. Despite its accuracy, this approach has a disadvantage in that it requires a large amount of quality-labeled data for the generation of models, which is difficult to obtain.

In [81] they introduced a method of CBMIR, where this method is composed of two phases: enrollment and querying. Firstly, the Discrete Wavelet Transform (DWT) coefficients were calculated for each inbound image with four types of Haar [82], [83], Daubechies [84]–[86], Coiflet Wavelets [87], and the most suitable type of wavelet for tested and compared retrieval system for each inbound image. Then, from wavelet coefficients, the Block Truncation Codes (BTCs) have been extracted. The suggested method was also enhanced with various scanning techniques. Rasters, zigzags, Morton, and Hilbert scans were used to split the image into subblocks to match BTC. The derived codes are then stored as a database of the feature vectors. Secondly, the BTCs are extracted from the wavelet coefficients of the query image during the query process. Eight different distance metrics were used to measure similarity. In order to test their method, three medical image databases were used, namely 7500 CT brain images collected from a teaching hospital in Egypt, Kvasir, and VIA-ELCAP

. The experimental results indicate that in contrast with other methods the method is very efficient in use. The proposed method also showed strong results in the extraction of Morton BTCs from the DB2 DWT analysis and the best estimation of similarities with the Manhattan distance. Given these benefits, but with some disadvantages, where the feature vector will be very large, in [74] have better accuracy on the Kvasir database than this method and the high computational complexity where this method searches the images in the whole database to compute the similarity.

In [88], a relevant feedback retrieval method (RFRM) for CBMIR has been suggested. Here the feedback is based on voting values performed in the image repository by each class, where a group of color features and texture was extracted using well-known color moments and GLCM texture features extraction methods and eight common coefficients of similarity were used as a base for similarity measures. After a rapid search using a single query that is taken randomly, the images that have top rank are selected from the dataset to determine the most efficient coefficient of similarity for the final search process. This method was applied to benchmark datasets the Kvasir dataset, and the PH2 dataset, where the experiments proved the superiority for improving the retrieval effectiveness of related medical images. Although this superiority, this method has a drawback, where it requires labeled data that are not easily available.

Because histological images gave a clear perspective of illnesses, the pathologist thought them to be the sole way to diagnose a disease. Automatic identification and extraction of advantageous traits from histopathological images can aid in the diagnosis, whereas manual assessment of microscopic images requires subjective pathologist interpretation and takes time. Therefore, a new CBMIR technique was introduced in [89]. The scheme presented downsamples the image to different scales, in which LTP is used for each downsampled image for lower, upper, and then divides into concentrated patches. The scheme defines the images on a different scale. In order to achieve the high accuracy of the retrieval of histopathological imagery, they have applied power-law normalization and a vector of locally aggregated descriptors (VLAD) to get the histogram images, which gives a high accuracy to the retrieval. The experiments have been conducted using the KIMIA Path960 dataset of standard 20-class histopathological data, and the results demonstrated that their method achieves better retrieval accuracy than other techniques. However, this technique has a drawback, as these require improvement from the computation complexity and performance.

In [90], an efficient and scalable histopathological image retrieval method was suggested for the learning of binary representation using densely connected multi-magnification hashing (DCMMH), where in contrast to earlier works, which focuses only on one magnifications level. So, this method cooperates with many magnification levels, to learn hashing functions based on CNNs. There is a reciprocal learning guidance model focusing on image data of high-low magnification pairs. To fully utilize cross-magnification information, a dense-connected architecture has been implemented. This method has been applied to two benchmark datasets BreakHis, and PLOSONE. In comparison to previous hasher methods based on handmade features, top performances were achieved in these experiments. So, this method contributed to decreasing clinician manual effort in diagnosis the histopathological images. However, the retrieval by cross-magnification is not available. Although the binary codes for histopathological images are employed by various magnification levels. Furthermore, computational complexity is increased.

Also, the histopathological image containing more information that can be used in the early detection of breast cancers and it's important to learn the compact representation to histopathological image retrieval. So, in [91], a new framework was presented for learning binary histopathologic image codes. This framework is multi-magnification correlation hashing (MMCH), in which both low-magnification and high-magnification data are used to learn discriminatory features. In particular, they built a patch-link graph with local patches extracted randomly from the labeled high-mag and low-mag images which is and propagated the link between high-mag images and low-mag patches to assess the semantic similarity of local patches. Similarities are then kept on the patch link graph and global labels to learn the binary codes of local patches. Additionally, $L_{2,1}$ hashing function restrictions have been introduced to pick from the original visual representation the more informative features, where $L_{2,1}$ constraints get better discrimination to the feature. They used BreakHis dataset, and PLOSONE dataset to perform the experiments, where experiments have shown that their method has improved accuracy through a series of cell-based and comprehensive approaches to histopathological image retrieval tasks. Despite all this improvement but this approach has a drawback, where distance computation time is $O(n^2)$, and the query is not as effective as holistic-based methods when data have high resolutions.

A Deep Convolutional Hash (DCH) method has been proposed in [92] for the encoding of images

in binary codes. There is an embedded LBE layer available on the proposed network and it may be trained "point-wise" way. The joint objective optimization function has also been constructed to encourage the network to learn discriminating representations from label information and decrease the gap between embedded features of low dimensions and necessary binary values. Binary encoding for new images has been provided through the network propagation and the quantification of the LBE layer output. This method has been applied to the histopathology image dataset which has been created by them including lung cancer images and skeletal muscle images. From the experiments, superior performances in the histopathology image dataset demonstrate the efficacy of this method. However, the optimization is currently eased through by the use of the non-linear (tanh) saturation function, which might restrict the efficiency of the binary codes learned. In addition, noise from labels would have a detrimental effect on model learning and ultimate disease diagnosis because no noise is assumed by the method on image labels.

In [93] suggested method for improving medical decision support systems, i.e. breast cancer diagnosis and including AL/RF in the medical imaging region, by utilizing the Medical Active leaRning and Retrieval (MARRow). In order to minimize many of the disadvantages in terms of efficiency and quality of the system, the commission introduced an AL Strategy that was suitably incorporated into the CBIR core mechanism. Since their AL strategy chooses a little more informative images based not just on the similarity, but also on the degree of uncertainty and diversity. These selected images will benefit from literature rather than those from the same class. This strategy has achieved a high improvement over the most advanced methods achieving a precision increase of up to 87.3%. MARRow also showed a clear and acceptable rate of growth over the course of the learning iterations. The time of the learning procedure is reduced by this method, as it eliminates the involvement of the expert in the analysis process (eliminates up to 88%) as the expert doesn't have to annotate (correct) the labels on all samples as needed by the work of literature. They make a more rigorous class approach (i.e. provide fewer misclassifications) as more information samples are chosen to learning. However, complexity is increased in this method by its intrinsic inter-class similarity which leads to the process of fine-grain annotations to make a more complicated difference between relevant and irrelevant pictures.

In [94] a similarity measurement method is suggested, which integrates deep features for a mammogram. The images are processed first in advance to extract low-level data, including content and location, but before extracting location features, the registration is done using the standard image. Then, the following are developed to extract the deep features that are regarded to be very effective: the Stacked Auto-Encoder Network (SAE), the Convolutional Neural Network (CNN), and the Deep Belief Network (DBN). The similarity of the contents and the deep similarities are computed using the ED among the query and the images in the dataset separately, however, for the similarity of the location, the intersection ratio to the mass regions is calculated. The similarity between content, location, and deep similarity is ultimately merged to form the image fusion similarity. This procedure has been applied to 740 cases of mammograms, which are 740 MLO mammograms from northeast china and their corresponding diagnostic reports. The experiments demonstrated the superiority in enhancing the efficacy of medical images retrieval and reducing the issue of the semantic gap. Although this superiority, this method has a high dimensional feature vector that will lead to increasing the computational complexity.

Individual features of a multi-phase CT image to indicate the region that is abnormal from the liver and apply it in an accurate retrieval of liver CT images were suggested in [95]. Two methods for retrieval of liver lesions were suggested. In the first method, for every imaging phase, individual features were selected to enhance the lesion class separability. In the second method, an 87×1 element vector was presented to represent different regions of an abnormal region. The correlation graph distance [96], which represents the feature vector's nonlinear structure, was also utilized to calculate the distance between an input image and other database images. Their method has been applied to 411 CT liver data consisting of three phases [97], [98]. From the experiments, has been demonstrated that the use of a manifold image distance measurement scheme enhances CBMIR 's discrimination efficiency. Furthermore, when compared to recent methods, a more complicated feature vector enhances the outcomes. and on average, the overall recall of their results with the proposed features vector was increased by 7.5%. However, this method needs additional features to replace the existing huge multi-phase data feature vector and needs to obtain a larger dataset and test the method's efficacy.

Due to their different fracture locations, the retrieval of bone images affected by avascular necrosis (AN) is difficult. So, an effective methodology for retrieving AN image using Deep Belief CNN

feature representation has been suggested in [99]. At first, pre-processing takes place for the input dataset. In addition, throughout the pre-processing step, image noise was eradicated with the use of the Median Filter (MF) and resized. Then, the features were transmuted to binary codes after being represented by the (DB-CNN). Ultimately, the calculation of the similarity was determined using the modified Hamming distance and retrieve the images. This method has been applied to the (Femur, Humerus, Knee) of the AN images dataset, where the experiments showed its superiority compared to the recent methods. However, it is limited to this dataset, and getting a large number of data for analysis is very difficult. So, the real data is very limited in this research.

In order to distinguish between normal and abnormal lung CT images, in [100] the local diagonal Laplacian pattern (LDLP) has been proposed as a novel low dimensional descriptor with computational efficiency. In order to define the diagonal neighbor center pixel relation, LDLP uses a derivative method of the second order. This had led to a feature vector of low-dimensional with rich local structure information and thus the calculation costs were significantly reduced. First, the feature histograms for the chest CT image slices of the EMPHYSEMA database were identified. Then the statistical method ANOVA was also used for measuring and analyzing the distance between normal and emphysematous tissue features. In addition, a classification of four-class has been produced using the classification of a neural artificial network. In the end, the results of the experiment have compared with prominent methods like LBP, local tetra pattern (LTrP) [101], local diagonal extrema pattern (LEDP) [46] and have been high accuracy compared with them. This method failed to fully extract the high-level semantic information.

As we viewed, the images are first identified and then categorized in the current methods and this resulted in increasing the period for image retrieval as the entire database must be searched for performing the retrieval. So, a Grey Wolf Optimization-Support Vector Machine (GWO-SVM) method was proposed in [102] which classifies the query image's class at first. In addition, only the query images database can organize the retrieval process. The GWO algorithm makes a distinctly improved value for the SVM classification for the solved and optimized parameters. Therefore, it is evident that the retrieval rate is high after the classification is performed relative to the current methods by defining the retrieval levels. This has been applied to 7641 medical CT images that including 27 classes of different body parts. Tests have shown superior accuracy classification with a 97% and improvement in the accuracy of retrieval compared to current methods. However, this method has a high dimensional feature vector which considers a drawback.

in [103] they have presented a new great power and reversible data concealing method for systems of electronic healthcare. To assure medical images reversibility, the conversion approach PTB (Pixel to Block) has been employed as a powerful and efficient alternative computationally to fulfill the cover image production. In order to verify the content at the receiver and simplify the tamper localization and detection, they have placed in the image cover a fragile watermark and Block Checksum (calculated for each block of 4×4). Also, to circumvent the attacks of widely used LSB removal, the data of checksum, watermark, and EPR were inserted using the ISBS (Intermediate Significant Bit Substitution). To improve data security, they have encrypted the data of EPR (Electronic Patient Record)/clinical and watermark by using the chaos of Non-linear dynamics. By applying the method to different image processing and geometric assaults, it was tested for imperceptibility of perceptual and the effectiveness of tamper detection. The experimental findings show that, in addition to being totally reversible, the suggested method is capable of producing high-quality watermarked images for a relatively large payload.

To allow any medical practitioner to obtain images in an encrypted domain in the cloud environment a secure healthcare CBIR for systems of medical image retrieval that depend on computational intelligence has been introduced in [104]. In this case, the only solution that adequately handles the comparison of the features that are encrypted is to make the similarity matching based on hamming distance. To achieve similarity matching, the binary features are utilized by this approach, which performs poorly in image retrieval. To improve the accuracy of the retrieval, they have proposed a technique that depends on salient components for binary feature extraction. Firstly, the input image has been rearranged to position the salient components at the beginning blocks using the saliency map, entropy, and primary texture direction. In order to get local binary features, they have used the strategy of block-level majority voting on the prominent blocks of the image. As a consequence, more features are obtained by the final feature vector from the image's prominent region, which enhances the accuracy of the retrieval. To fulfill the security element, they have made retrieval of the image in the cloud environment, which includes the Database Service Provider, Data Owner, and Client across the encrypted domain and the binary feature vector also has encrypted.

TABLE I: Summarization of mentioned methods in terms of the model, the dataset used by each method, classification technique applied to the dataset, feature vector length, extraction and retrieval time, and the accuracy of the model for each dataset.

Paper	Model	Dataset	Classification Technique	Feature Length	Extraction Time in(s)	Retrieval Time in(s)	Accuracy(%) ARP	ARR	F-measure	mAP
[46]	LWP	NEMA-CT	Manually	256	98.25	0.45	95.32 @10	31.33 @10	47.16 @10	-
		EXACT09-CT		256	~150	~ 1	83.00 @10	24.87 @10	38.27 @10	-
		TCIA-CT		256	~140	~0.8	88.42 @10	13.09 @10	22.8 @10	-
[50]	HCSCs	NEMA-CT	Manually	200	384.1	-	98.33 @10	33.64 @10	50.13 @10	-
		EXACT09-CT		200	384.1	-	91.50 @10	28.83 @10	43.84 @10	-
		TCIA-CT		200	384.1	-	95.12 @10	14.52 @10	25.20 @10	-
[52]	Filtering+ Partitioning+BoW	EXACT09-CT	Manually	-	-	-	92.97 @10	29.31 @10	44.57 @10	-
		TCIA-CT		-	-	-	96.32 @10	14.67 @10	25.46 @10	-
[53]	*ST–DCavg*	EXACT09-CT	Manually	200	384.1	-	92.09 @10	29.07 @10	44.19 @10	-
	ST–DCmax	EXACT09-CT		200	384.1	-	91.93 @10	28.98 @10	44.07 @10	-
	ST–CCAh	EXACT09-CT		-	14.98	-	91.92 @10	28.90 @10	43.98 @10	-
	ST–CCAv	EXACT09-CT		-	14.98	-	93.35 @10	29.44 @10	44.76 @10	-
	ST–DCavg	TCIA-CT		200	384.1	-	95.80 @10	14.65 @10	25.41 @10	-
	ST–DCmax	TCIA-CT		200	384.1	-	95.71 @10	14.58 @10	25.30 @10	-
	ST–CCAh	TCIA-CT		-	14.98	-	96.33 @10	14.68 @10	25.48 @10	-
	ST–CCAv	TCIA-CT		-	14.98	-	96.45 @10	14.71 @10	25.52 @10	-
[46]	LBDP	Emphysema-CT	Manually	256	2.39	0.06	~50@100	~89.5 @100	~64.2 @100	-
		NEMA-CT		256	606.20	0.43	99.55 @5	75.83 @50	67.64 @50	-
		OASIS-MRI		256	56.78	0.33	~58 @10	~24 @10	~34 @10	-
[54]	LMVCoP	OASIS-MRI	Manually	-	4.29	0.21	87.57 @10	53.21 @10	61.04 @10	-
[57]	(*MD*)2MaMEP	MESSIDOR	Manually	2560	-	-	56.93 @5	-	-	-
		OASIS MRI		2560	-	-	62.49 @10	-	-	-
		VIA/I-ELCAP		2560	-	-	93.36 @10	60.40 @10	73.35 @10	-
[58]	CNN+PL	NEMA-CT	Manually	4096	-	-	~90 @50	~69 @50	~78 @50	-
	SDAE+PL	NEMA-CT		256	7.77	3.72	~90 @50	~69 @50	~78 @50	-
	CNN+PL	OASIS-MRI		4096	-	-	68.8 @50	32.8 @50	44.4 @50	-
	SDAE+PL	OASIS-MRI		256	2.88	3.11	61.1 @50	28.9 @50	39.24 @50	-
	CNN+PL	TCIA-CT		4096	-	-	~90 @50	~58 @50	~70 @50	-
	SDAE+PL	TCIA-CT		256	6.24	4.50	91 @50	59.1 @50	71.7 @50	-
[59]	ZMs	Emphysema-CT	Manually	12	0.85	0.24	44.88 @100	79.48 @100	57.37 @100	60.23 @100
		Noisy Emphysema-CT					43.90 @100	78.50 @100	56.39 @100	59.16 @100
		OASIS-MRI	Manually	12	16.85	1.37	42.81 @100	40.52 @100	41.63 @100	49.41 @100
		Noisy OASIS-MRI					42.39 @100	39.54 @100	41.50 @100	48.72 @100
[63]	OFFMs	Emphysema-CT	Manually	16	0.26	0.11	45.31 @100	80.34 @100	57.94 @100	62.35 @100
		Noisy Emphysema-CT					45.03 @100	79.82 @100	57.58 @100	62.39 @100
		NEMA-CT	Manually	16	65.42	1.46	68.03 @100	97.24 @100	80.05 @100	99.12 @100
		Noisy NEMA-CT					48.51 @100	74.12 @100	58.64 @100	76.52 @100
		OASIS-MRI	Manually	16	7.49	0.67	42.52 @100	40.17 @100	41.31 @100	51.09 @100
		Noisy OASIS-MRI					33.76 @100	30.39 @100	31.98 @100	35.75 @100
		NEMA-MR	Manually	16	10.14	1.17	80.30 @100	100.00 @100	89.07 @100	100.00 @100
		Noisy NEMA-MR					56.82 @100	76.32 @100	65.14 @100	78.82 @100
[64]	ANTIC	MESSIDOR	Manually	2048	-	-	-	~54 @10	-	-
		NEMA-CT		2048	-	-	96.79 @10	-	-	-
		OASIS MRI		2048	-	-	~56.5 @10	-	-	-
		VIA/I-ELCAP		2048	-	-	~91 @10	~9 @10	~16.38 @10	-
[65]	LDEBP+ LZMs	Emphysema-CT	Manually	85	11.85	0.49	~52 @100	~87 @100	~65 @100	-
		OASIS-MRI		85	23.51	1.95	71.08 @100	30.41 @100	42.6 @100	-
		Brain-Tumor		85	185.72	2.81		~51 @100	-	-
[67]	TLBAP + LANADP	NEMA-CT	Manually	512	-	0.1160	96.34 @10	11.76 @10	20.96 @10	-
		OASIS-MRI		512	-	0.0714	63.39 @10	58.11 @10	60.64 @10	-
		VIA/I-ELCAP		512	-	0.1760	43.80 @100	43.81 @100	41.44 @100	-
[68]	Siamese network+ hash coding	TCIA-CT [69]	Siamese network+ hash coding	48-bits	-	0.382952	-	-	-	~80 @100
		VIA/I-ELCAP		48-bits	-	0.382952	85.7 @50	-	-	81.63 @100
[70]	IR-Net	OASIS-MRI	Manually	512	-	-	70.45 @10	-	-	-
		VIA/I-ELCAP		512	-	-	99.36 @10	99.36 @10	99.36 @10	-
		ILD		512	-	-	80.87 @10	-	-	-
[71]	3D-LOZFP	NEMA-CT	Manually	192	1.73	-	84.37 @30	69.30 @30	76.1 @30	-
		TCIA-CT		192	1.73	-	93.17 @30	63.36 @30	75.43 @30	-
[72]	deep hashing	LIDC-IDRI	Radiologists	64	-	-	-	-	-	63.51@100
[73]	DCNN	Multimodal	DCNN	4096	-	-	71.50 @21	-	-	69@21
[74]	AlexNet and SMAP	Kvasir	SVM	96	-	-	74.02 @50	-	-	-

To be continued

TABLE I (continued)

Paper	Model	Dataset	Classification Technique	Feature Length	Extraction Time in(s)	Retrieval Time in(s)	Accuracy(%) APR	ARR	F-measure	mAP
[75]	CNN and FFT	Kvasir	-	128-bits	-	-	46.5 @50	-	-	-
		IRMA 2009		128-bits	-	-	77.00 @50	-	-	-
[79]	BoVW and SSI	Multimodal	BoVW	-	-	-	80.50 @21	-	-	69.70 @21
		Kvasir		-	-	-	60.48 @50	-	-	-
		IRMA 2009		-	-	-	83.9 @50	-	-	-
[80]	Topic and Location	Multimodal	Topic and Location	24	-	-	88.75 @21	-	-	86.74 @21
		IRMA 2009		57	-	-	97.5 @10	-	-	-
[81]	DWT+ BTCs	Kvasir	Manually	-	-	-	55.3 @50	-	-	-
		VIA/I-ELCAP	-	-	-	-	86.7 @50	-	-	-
[88]	RFRM	Kvasir	Medical Experts	18	-	-	85@10	-	-	-
[89]	LTP +VLAD	KIMIA	Manually	-	-	-	95 @10	20.21 @10	33.33 @10	-
		Path960		-	-	-	84.65 @20	36.02 @20	50.71 @20	-
[90]	DCMMH-All (40-100-200-400)	BreakHis 40×	Manually	16-bit	-	-	-	-	-	95.41 @5
		BreakHis 100×		16-bit	-	-	-	-	-	93.12 @5
		BreakHis 200×		16-bit	-	-	-	-	-	96.55 @5
		BreakHis 400×		16-bit	-	-	-	-	-	95.14 @5
	DCMMH	PLOSONE 200×		64-bit	-	-	-	-	-	32.46 @5
[91]	MCCH-40-200	BreakHis 40×	Manually	16-bit	-	-	-	-	-	92.52 @5
	MCCH-100-200	BreakHis 100×		16-bit	-	-	-	-	-	91.52 @5
	MCCH-200-400	BreakHis 200×		16-bit	-	-	-	-	-	89.74 @5
	MCCH-200-400	BreakHis 400×		16-bit	-	-	-	-	-	88.76 @5
	MCCH	PLOSONE 100×		64-bit	-	-	-	-	-	55.76 @5
	MCCH	PLOSONE 200×		64-bit	-	-	-	-	-	54.19 @5
[92]	DCH	Skeletal Muscle+ lung cancer	Manually	64-bit	-	-	-	-	-	96 @1000
[93]	LBP-JD	*I*1-VIENNA	K-NN K-means	108	-	-	~93.7 @30	-	-	97.0 @30
	LBP-*L*2	*I*2-MIAS		108	-	-	100 @30	-	-	99.7 @30
	Zernike-*X*2	*I*3-DDSM		36	-	-	~49.4 @30	-	-	53.3 @30
	Zernike-*X*2	*I*4-MIAS-DDSM		36	-	-	~49.1 @30	-	-	52.7 @30
	Daubechies -$L\infty$	*I*5-VIENNA-DDSM		16	-	-	~61.6 @30	-	-	63.1 @30
[94]	GLCM+Tamura+ Hu Moment+ Gray Level Histogram+DBN	MLO mammograms	Manually	-	-	-	74.5 @15	85 @15	79.4 @15	-
[95]	manifold learning	CT liver data	Manually	87	-	16	P=83.6	R=84.2	83.9	-
[99]	DB-CNN	Femur images	Manually	-	-	11	P=92.3	R=81.56	86.6	-
		Humerus images		-	-	9	P=87.38	R=80.23	83.65	-
		Knee images		-	-	7	P=80.5	R=79.9	80.2	-
[100]	LDLP	Emphysema-CT Slice	Manually	25-bits	-	-	P=84.21	R=96.67	90.01	-
[102]	GWO-SVM	CT scan	GWO-SVM	-	-	-	-	-	-	90

To meet the security need, they have made image retrieval in the cloud environment, which includes the Database Service Provider, Data Owner, and Client across the encrypted domain, and the binary feature vector has also been encrypted. Finally, they have validated the accuracy performance of the retrieval of the proposed technique using medical and Corel images datasets. The experimental findings using real-life datasets show that the suggested technique is secure and delivers comparable retrieval accuracy to other analogous systems in the domain.

IV. **CONCLUSION**

In this survey, we have provided many datasets for medical images of various modalities (MR, CT, PT, PET, OPT, X-ray, etc.) in addition to histopathological images and endoscopic images, and other modalities. The survey explained how state-of-the-art CBMIR methods have been applied to these datasets and how succeeded to achieve high accuracy, reduce the problem of the semantic gap, and resolving privacy-preserving by securing the retrieval method of medical images. Also, it is mentioned the relationship of methods to each other and how each method has been improved the retrieval better than other methods and compared the results of all methods on this dataset. In addition to mentioning the advantages and disadvantages of each method. As we view, there are many challenges facing the process of retrieval and securing the retrieval of medical images from large repositories. So, we wish that our survey helps the researchers to Look at the disadvantages

and exploit the comparisons in the table between the state-of-the-art CBMIR methods and try to improve them and provide the best CBMIR.

REFERENCES

[1] M. Mizotin, J. Benois-Pineau, M. Allard, and G. Catheline, "Feature-based brain mri retrieval for alzheimer disease diagnosis," in 2012 19th IEEE International Conference on Image Processing. IEEE, 2012, pp. 1241–1244.

[2] G. W. Jiji and P. S. J. D. Raj, "Content-based image retrieval in dermatology using intelligent technique," IET Image Processing, vol. 9, no. 4, pp. 306–317, 2015.

[3] M. Ponciano-Silva, J. P. Souza, P. H. Bugatti, M. V. Bedo, D. S. Kaster, R. T. Braga, A. D. Bellucci, P. M. Azevedo-Marques, C. Traina, and A. J. Traina, "Does a cbir system really impact decisions of physicians in a clinical environment?" in Proceedings of the 26th IEEE International Symposium on Computer-Based Medical Systems. IEEE, 2013, pp. 41–46.

[4] G. Quellec, M. Lamard, G. Cazuguel, B. Cochener, and C. Roux, "Fast wavelet-based image characterization for highly adaptive image retrieval," IEEE Transactions on Image Processing, vol. 21, no. 4, pp. 1613–1623, 2011.

[5] M. M. Rahman, S. K. Antani, and G. R. Thoma, "A learning-based similarity fusion and filtering approach for biomedical image retrieval using svm classification and relevance feedback," IEEE Transactions on Information Technology in Biomedicine, vol. 15, no. 4, pp. 640–646, 2011.

[6] P. Welter, T. M. Deserno, B. Fischer, R. W. G¨unther, and C. Spreckelsen, "Towards case-based medical learning in radiological decision making using content-based image retrieval," BMC medical informatics and decision making, vol. 11, no. 1, pp. 1–16, 2011.

[7] Y. Liu, D. Zhang, G. Lu, and W.-Y. Ma, "A survey of content-based image retrieval with high-level semantics," Pattern recognition, vol. 40, no. 1, pp. 262–282, 2007.

[8] J. Wan, D. Wang, S. C. H. Hoi, P. Wu, J. Zhu, Y. Zhang, and J. Li, "Deep learning for content-based image retrieval: A comprehensive study," in Proceedings of the 22nd ACM international conference on Multimedia, 2014, pp. 157–166.

[9] K. K. Kumar and T. V. Gopal, "A novel approach to self order feature reweighting in cbir to reduce semantic gap using relevance feedback," in 2014 International Conference on Circuits, Power and Computing Technologies [ICCPCT-2014]. IEEE, 2014, pp. 1437–1442.

[10] Y. Bengio, A. C. Courville, and P. Vincent, "Unsupervised feature learning and deep learning: A review and new perspectives," CoRR, abs/1206.5538, vol. 1, p. 2012, 2012.

[11] G. Antonellis, A. G. Gavras, M. Panagiotou, B. L. Kutter, G. Guerrini, A. C. Sander, and P. J. Fox, "Shake table test of large-scale bridge columns supported on rocking shallow foundations," Journal of Geotechnical and Geoenvironmental Engineering, vol. 141, no. 5, p. 04015009, 2015.

[12] M. D. Zeiler and R. Fergus, "Visualizing and understanding convolutional networks," in European conference on computer vision. Springer, 2014, pp. 818–833.

[13] A. Karpathy, G. Toderici, S. Shetty, T. Leung, R. Sukthankar, and L. Fei-Fei, "Large-scale video classification with convolutional neural networks," in Proceedings of the IEEE conference on Computer Vision and Pattern Recognition, 2014, pp. 1725–1732.

[14] G. Wu, W. Lu, G. Gao, C. Zhao, and J. Liu, "Regional deep learning model for visual tracking," Neurocomputing, vol. 175, pp. 310–323, 2016.

[15] G. Hinton, L. Deng, D. Yu, G. E. Dahl, A.-r. Mohamed, N. Jaitly, A. Senior, V. Vanhoucke, P. Nguyen, T. N. Sainath et al., "Deep neural networks for acoustic modeling in speech recognition: The shared views of four research groups," IEEE Signal processing magazine, vol. 29, no. 6, pp. 82–97, 2012.

[16] S. Zhou, Q. Chen, and X. Wang, "Active deep learning method for semi-supervised sentiment classification," Neurocomputing, vol. 120, pp. 536–546, 2013.

[17] A. K. Jain and A. Vailaya, "Image retrieval using color and shape," Pattern recognition, vol. 29, no. 8, pp. 1233–1244, 1996.

[18] B. S. Manjunath and W.-Y. Ma, "Texture features for browsing and retrieval of image data," IEEE Transactions on pattern analysis and machine intelligence, vol. 18, no. 8, pp. 837–842, 1996.

[19] J. P. Eakins, "Towards intelligent image retrieval," Pattern Recognition, vol. 35, no. 1, pp. 3–14, 2002.

[20] D. G. Lowe, "Object recognition from local scale-invariant features," in Proceedings of the seventh IEEE international conference on computer vision, vol. 2. Ieee, 1999, pp. 1150–1157.

[21] H. Bay, A. Ess, T. Tuytelaars, and L. Van Gool, "Speeded-up robust features (surf)," Computer vision and image understanding, vol. 110, no. 3, pp. 346–359, 2008.

[22] J. Yang, Y.-G. Jiang, A. G. Hauptmann, and C.-W. Ngo, "Evaluating bag-of-visual-words representations in scene classification," in Proceedings of the international workshop on Workshop on multimedia information retrieval, 2007, pp. 197–206.

[23] J. Sivic, B. C. Russell, A. A. Efros, A. Zisserman, and W. T. Freeman, "Discovering objects and their location in images," in Tenth IEEE International Conference on Computer Vision (ICCV'05) Volume 1, vol. 1. IEEE, 2005, pp. 370–377.

[24] L. Wu and S. C. Hoi, "Enhancing bag-of-words models with semantics-preserving metric learning," IEEE MultiMedia, vol. 18, no. 1, pp. 24–37, 2011.

[25] X. Wangming, W. Jin, L. Xinhai, Z. Lei, and S. Gang, "Application of image sift features to the context of cbir," in 2008 International Conference on Computer Science and Software Engineering, vol. 4. IEEE, 2008, pp. 552–555.

[26] Z. Mansoori and M. Jamzad, "Content based image retrieval using the knowledge of texture, color and binary tree structure," in 2009 Canadian Conference on Electrical and Computer Engineering. IEEE, 2009, pp. 999–1003.

[27] A. Alfanindya, N. Hashim, and C. Eswaran, "Content based image retrieval and classification using speeded-up robust features (surf) and grouped bag-of-visual-words (gbovw)," in 2013 International Conference on Technology, Informatics, Management, Engineering and Environment. IEEE, 2013, pp. 77–82.

[28] E. Decenci`ere, X. Zhang, G. Cazuguel, B. Lay, B. Cochener, C. Trone, P. Gain, R. Ordonez, P. Massin, A. Erginay et al., "Feedback on a publicly distributed image database: the messidor database," Image Analysis & Stereology, vol. 33, no. 3, pp. 231–234, 2014.

[29] knee image . (2004) [online]. [Online]. Available: http://www.osirix-viewer.com/datasets/DATA/KNEE.zip

[30] K. Pogorelov, K. R. Randel, C. Griwodz, S. L. Eskeland, T. de Lange, D. Johansen, C. Spampinato, D.-T. Dang-Nguyen, M. Lux, P. T. Schmidt et al., "Kvasir: A multi-class image dataset for computer aided gastrointestinal disease detection," in Proceedings of the 8th ACM on Multimedia Systems Conference, 2017, pp. 164–169.
[31] Emphysema-CT Database. (2010) [online]. [Online]. Available: https://lauge-soerensen.github.io/emphysema-database/
[32] NEMA-CT Database. (2012) [online]. [Online]. Available: ftp://medical.nema.org/medical/Dicom/Multiframe/CT
[33] S. R. Dubey, S. K. Singh, and R. K. Singh, "Local wavelet pattern: A new feature descriptor for image retrieval in medical CT databases," IEEE Transactions on Image Processing, vol. 24, no. 12, pp. 5892–5903, dec 2015.
[34] K. Clark, B. Vendt, K. Smith, J. Freymann, J. Kirby, P. Koppel, S. Moore, S. Phillips, D. Maffitt, M. Pringle, L. Tarbox, and F. Prior, "The cancer imaging archive (TCIA): Maintaining and operating a public information repository," Journal of Digital Imaging, vol. 26, no. 6, pp. 1045–1057, jul 2013.
[35] NEMA-MR Database. (2012) [online]. [Online]. Available: ftp://medical.nema.org/medical/Dicom/Multiframe/MR
[36] OASIS-MRI Database. (2007) [online]. [Online]. Available: http://www.oasis-brains.org/
[37] M. D. Kumar, M. Babaie, S. Zhu, S. Kalra, and H. R. Tizhoosh, "A comparative study of cnn, bovw and lbp for classification of histopathological images," in 2017 IEEE Symposium Series on Computational Intelligence (SSCI). IEEE, 2017, pp. 1–7.
[38] VIA/I-ELCAP Database. (2003) [online]. [Online]. Available: http://www.via.cornell.edu/lungdb.html
[39] P. Lo, B. Van Ginneken, J. M. Reinhardt, T. Yavarna, P. A. De Jong, B. Irving, C. Fetita, M. Ortner, R. Pinho, J. Sijbers et al., "Extraction of airways from ct (exact'09)," IEEE Transactions on Medical Imaging, vol. 31, no. 11, pp. 2093–2107, 2012.
[40] F. A. Spanhol, L. S. Oliveira, C. Petitjean, and L. Heutte, "A dataset for breast cancer histopathological image classification," Ieee transactions on biomedical engineering, vol. 63, no. 7, pp. 1455–1462, 2015.
[41] T. Ara´ujo, G. Aresta, E. Castro, J. Rouco, P. Aguiar, C. Eloy, A. Pol´onia, and A. Campilho, "Classification of breast cancer histology images using convolutional neural networks," PloS one, vol. 12, no. 6, p. e0177544, 2017.
[42] P. H. Oliveira, L. C. Scabora, M. T. Cazzolato, M. V. Bedo, A. J. Traina, and C. Traina-Jr, "Mammoset: An enhanced dataset of mammograms," in Proc. Satellite Events 32nd Brazilian Symp. Databases, 2017, pp. 256–266.
[43] A. Depeursinge, A. Vargas, A. Platon, A. Geissbuhler, P.-A. Poletti, and H. M¨uller, "Building a reference multimedia database for interstitial lung diseases," Computerized medical imaging and graphics, vol. 36, no. 3, pp. 227–238, 2012.
[44] Brain-Tumor Database. (2017) [online]. [Online]. Available: https://figshare.com/articles/brain_tumor_dataset/1512427/5
[45] S. G. Armato III, G. McLennan, L. Bidaut, M. F. McNitt-Gray, C. R. Meyer, A. P. Reeves, B. Zhao, D. R. Aberle, C. I. Henschke, E. A. Hoffman et al., "The lung image database consortium (lidc) and image database resource initiative (idri): a completed reference database of lung nodules on ct scans," Medical physics, vol. 38, no. 2, pp. 915–931, 2011.
[46] S. R. Dubey, S. K. Singh, and R. K. Singh, "Local wavelet pattern: a new feature descriptor for image retrieval in medical ct databases," IEEE Transactions on Image Processing, vol. 24, no. 12, pp. 5892–5903, 2015.
[47] X. Tan and B. Triggs, "Enhanced local texture feature sets for face recognition under difficult lighting conditions," IEEE transactions on image processing, vol. 19, no. 6, pp. 1635–1650, 2010.
[48] S. Murala and Q. J. Wu, "Local ternary co-occurrence patterns: a new feature descriptor for mri and ct image retrieval," Neurocomputing, vol. 119, pp. 399–412, 2013.
[49] T. Ojala, M. Pietikainen, and T. Maenpaa, "Multiresolution gray-scale and rotation invariant texture classification with local binary patterns," IEEE Transactions on pattern analysis and machine intelligence, vol. 24, no. 7, pp. 971–987, 2002.
[50] R. Lan and Y. Zhou, "Medical image retrieval via histogram of compressed scattering coefficients," IEEE journal of biomedical and health informatics, vol. 21, no. 5, pp. 1338–1346, 2016.
[51] S. Murala and Q. J. Wu, "Spherical symmetric 3d local ternary patterns for natural, texture and biomedical image indexing and retrieval," Neurocomputing, vol. 149, pp. 1502–1514, 2015.
[52] R. Lan, S. Zhong, Z. Liu, Z. Shi, and X. Luo, "A simple texture feature for retrieval of medical images," Multimedia Tools and Applications, vol. 77, no. 9, pp. 10853–10866, 2018.
[53] R. Lan, H. Wang, S. Zhong, Z. Liu, and X. Luo, "An integrated scattering feature with application to medical image retrieval," Computers & Electrical Engineering, vol. 69, pp. 669–675, 2018.
[54] A. Jenitta and R. S. Ravindran, "Image retrieval based on local mesh vector co-occurrence pattern for medical diagnosis from mri brain images," Journal of medical systems, vol. 41, no. 10, pp. 1–10, 2017.
[55] R. M. Haralick, K. Shanmugam, and I. H. Dinstein, "Textural features for image classification," IEEE Transactions on systems, man, and cybernetics, no. 6, pp. 610–621, 1973.
[56] K.-C. Fan and T.-Y. Hung, "A novel local pattern descriptor—local vector pattern in high-order derivative space for face recognition," IEEE transactions on image processing, vol. 23, no. 7, pp. 2877–2891, 2014.
[57] G. Galshetwar, L. M. Waghmare, A. B. Gonde, and S. Murala, "Multi-dimensional multi-directional mask maximum edge pattern for bio-medical image retrieval," International Journal of Multimedia Information Retrieval, vol. 7, no. 4, pp. 231–239, 2018.
[58] S. Pang, M. A. Orgun, and Z. Yu, "A novel biomedical image indexing and retrieval system via deep preference learning," Computer methods and programs in biomedicine, vol. 158, pp. 53–69, 2018.
[59] Y. Kumar, A. Aggarwal, S. Tiwari, and K. Singh, "An efficient and robust approach for biomedical image retrieval using zernike moments," Biomedical Signal Processing and Control, vol. 39, pp. 459–473, 2018.
[60] M. R. Teague, "Image analysis via the general theory of moments," Josa, vol. 70, no. 8, pp. 920–930, 1980.
[61] S. Murala and Q. J. Wu, "Mri and ct image indexing and retrieval using local mesh peak valley edge patterns," Signal processing: image communication, vol. 29, no. 3, pp. 400–409, 2014.
[62] M. Verma and B. Raman, "Center symmetric local binary co-occurrence pattern for texture, face and bio-medical image retrieval," Journal of Visual Communication and Image Representation, vol. 32, pp. 224–236, 2015.
[63] A. Aggarwal, S. Sharma, K. Singh, H. Singh, and S. Kumar, "A new approach for effective retrieval and indexing of medical images," Biomedical Signal Processing and Control, vol. 50, pp. 10–34, 2019.

[64] M. Mandal, M. Chaudhary, S. K. Vipparthi, S. Murala, A. B. Gonde, and S. K. Nagar, "Antic: Antithetic isomeric cluster patterns for medical image retrieval and change detection," IET Computer Vision, vol. 13, no. 1, pp. 31–43, 2019.
[65] G. Sucharitha and R. K. Senapati, "Biomedical image retrieval by using local directional edge binary patterns and zernike moments," Multimedia Tools and Applications, vol. 79, no. 3, pp. 1847–1864, 2020.
[66] G. Sucharitha and R. K. Senapati, "Shape based image retrieval using lower order zernike moments," International Journal of Electrical and Computer Engineering, vol. 7, no. 3, p. 1651, 2017.
[67] R. Biswas, S. Roy, and D. Purkayastha, "An efficient content-based medical image indexing and retrieval using local texture feature descriptors," International Journal of Multimedia Information Retrieval, vol. 8, no. 4, pp. 217–231, 2019.
[68] Y. Cai, Y. Li, C. Qiu, J. Ma, and X. Gao, "Medical image retrieval based on convolutional neural network and supervised hashing," IEEE Access, vol. 7, pp. 51877–51885, 2019.
[69] TCIA-CT Database. (2010) [online]. [Online]. Available: https://wiki.cancerimagingarchive.net/display/Public/Wiki
[70] R. Pinapatruni and C. S. Bindu, "Learning image representation from image reconstruction for a content-based medical image retrieval," Signal, Image and Video Processing, pp. 1–8, 2020.
[71] R. Hatibaruah, V. K. Nath, and D. Hazarika, "Biomedical ct image retrieval using 3d local oriented zigzag fused pattern," in 2020 National Conference on Communications (NCC). IEEE, 2020, pp. 1–6.
[72] Y. Qi, J. Gu, Y. Zhang, G. Wu, and F. Wang, "Supervised deep semantics-preserving hashing for real-time pulmonary nodule image retrieval," Journal of Real-Time Image Processing, vol. 17, no. 6, pp. 1857–1868, 2020.
[73] A. Qayyum, S. M. Anwar, M. Awais, and M. Majid, "Medical image retrieval using deep convolutional neural network," Neurocomputing, vol. 266, pp. 8–20, 2017.
[74] J. Ahmad, K. Muhammad, M. Y. Lee, and S. W. Baik, "Endoscopic image classification and retrieval using clustered convolutional features," Journal of medical systems, vol. 41, no. 12, pp. 1–12, 2017.
[75] J. Ahmad, K. Muhammad, and S. W. Baik, "Medical image retrieval with compact binary codes generated in frequency domain using highly reactive convolutional features," Journal of medical systems, vol. 42, no. 2, pp. 1–19, 2018.
[76] J.-P. Heo, Y. Lee, J. He, S.-F. Chang, and S.-E. Yoon, "Spherical hashing," in 2012 IEEE Conference on Computer Vision and Pattern Recognition. IEEE, 2012, pp. 2957–2964.
[77] Z. Jin, C. Li, Y. Lin, and D. Cai, "Density sensitive hashing," IEEE transactions on cybernetics, vol. 44, no. 8, pp. 1362–1371, 2013.
[78] Y. Gong, S. Lazebnik, A. Gordo, and F. Perronnin, "Iterative quantization: A procrustean approach to learning binary codes for large-scale image retrieval," IEEE transactions on pattern analysis and machine intelligence, vol. 35, no. 12, pp. 2916–2929, 2012.
[79] P. Shamna, V. Govindan, and K. A. Nazeer, "Content-based medical image retrieval by spatial matching of visual words," Journal of King Saud University-Computer and Information Sciences, 2018.
[80] P. Shamna, V. Govindan, "Content based medical image retrieval using topic and location model," Journal of biomedical informatics, vol. 91, p. 103112, 2019.
[81] H. Kasban and D. Salama, "A robust medical image retrieval system based on wavelet optimization and adaptive block truncation coding," Multimedia Tools and Applications, vol. 78, no. 24, pp. 35211–35236, 2019.
[82] S. Arora, Y. S. Brar, and S. Kumar, "Haar wavelet transform for solution of image retrieval," signal, vol. 2, no. 2, p. 1, 2001.
[83] K. A. Bhandari and R. M. Ramchandra, "An innovative remote sensing image retrieval techniques based on haar wavelet-ltrp and anfis," Procedia Computer Science, vol. 79, pp. 391–401, 2016.
[84] D. A. Chandy, A. H. Christinal, A. J. Theodore, and S. E. Selvan, "Neighbourhood search feature selection method for content-based mammogram retrieval," Medical & biological engineering & computing, vol. 55, no. 3, pp. 493–505, 2017.
[85] J. Z. Wang, G. Wiederhold, O. Firschein, and S. X. Wei, "Content-based image indexing and searching using daubechies' wavelets," International Journal on Digital Libraries, vol. 1, no. 4, pp. 311–328, 1998.
[86] E. Yildizer, A. M. Balci, T. N. Jarada, and R. Alhajj, "Integrating wavelets with clustering and indexing for effective content-based image retrieval," Knowledge-Based Systems, vol. 31, pp. 55–66, 2012.
[87] K. Jaspreet and K. Rajneet, "Biomedical image denoising using symlet wavelet with wiener filter," Int. J. Eng. Res. Appl, vol. 3, pp. 548–550, 2013.
[88] A. Ahmed, "Implementing relevance feedback for content-based medical image retrieval," IEEE Access, vol. 8, pp. 79969–79976, 2020.
[89] K. N. Sukhia, M. M. Riaz, A. Ghafoor, S. S. Ali, and N. Iltaf, "Content-based histopathological image retrieval using multi-scale and multichannel decoder based ltp," Biomedical Signal Processing and Control, vol. 54, p. 101582, 2019.
[90] Y. Gu and J. Yang, "Densely-connected multi-magnification hashing for histopathological image retrieval," IEEE journal of biomedical and health informatics, vol. 23, no. 4, pp. 1683–1691, 2018.
[91] Y. Gu and J. Yang, "Multi-level magnification correlation hashing for scalable histopathological image retrieval," Neurocomputing, vol. 351, pp. 134–145, 2019.
[92] M. Sapkota, X. Shi, F. Xing, and L. Yang, "Deep convolutional hashing for low-dimensional binary embedding of histopathological images," IEEE journal of biomedical and health informatics, vol. 23, no. 2, pp. 805–816, 2018.
[93] R. S. Bressan, P. H. Bugatti, and P. T. Saito, "Breast cancer diagnosis through active learning in content-based image retrieval," Neurocomputing, vol. 357, pp. 1–10, 2019.
[94] Z. Wang, J. Xin, Y. Huang, L. Xu, J. Ren, H. Zhang, W. Qian, X. Zhang, and J. Liu, "A similarity measure method fusing deep feature for mammogram retrieval," Journal of X-ray science and technology, vol. 28, no. 1, pp. 17–33, 2020.
[95] M. S. Mirasadi and A. H. Foruzan, "Content-based medical image retrieval of ct images of liver lesions using manifold learning," International Journal of Multimedia Information Retrieval, vol. 8, no. 4, pp. 233–240, 2019.
[96] S. Roy, Y. Chi, J. Liu, S. K. Venkatesh, and M. S. Brown, "Three-dimensional spatiotemporal features for fast content-based retrieval of focal liver lesions," IEEE Transactions on Biomedical Engineering, vol. 61, no. 11, pp. 2768–2778, 2014.
[97] J. Wang, J. Li, X.-H. Han, L. Lin, H. Hu, Y. Xu, Q. Chen, Y. Iwamoto, and Y.-W. Chen, "Tensor-based sparse representations of multi-phase medical images for classification of focal liver lesions," Pattern Recognition Letters, vol. 130, pp. 207–215, 2020.
[98] Y. Xu, L. Lin, H. Hu, D. Wang, W. Zhu, J. Wang, X.-H. Han, and Y.-W. Chen, "Texture-specific bag of visual words model and spatial cone matching-based method for the retrieval of focal liver lesions using multiphase

contrast-enhanced ct images," International journal of computer assisted radiology and surgery, vol. 13, no. 1, pp. 151–164, 2018.
[99] S. K. Sundararajan, B. Sankaragomathi, and D. S. Priya, "Deep belief cnn feature representation based content based image retrieval for medical images," Journal of medical systems, vol. 43, no. 6, pp. 1–9, 2019.
[100] P. K. R. Yelampalli, J. Nayak, and V. H. Gaidhane, "A novel binary feature descriptor to discriminate normal and abnormal chest ct images using dissimilarity measures," Pattern Analysis and Applications, vol. 22, no. 4, pp. 1517–1526, 2019.
[101] S. Murala, R. Maheshwari, and R. Balasubramanian, "Local tetra patterns: a new feature descriptor for content-based image retrieval," IEEE transactions on image processing, vol. 21, no. 5, pp. 2874–2886, 2012.
[102] R. D. Benyl and C. C. Seldev, "Novel real time content based medical image retrieval scheme with gwo-svm," Multimedia Tools and Applications, vol. 79, no. 23-24, pp. 17227–17243, 2020.
[103] S. A. Parah, F. Ahad, J. A. Sheikh, and G. Bhat, "Hiding clinical information in medical images: A new high capacity and reversible data hiding technique," Journal of Biomedical Informatics, vol. 66, pp. 214–230, feb 2017.
[104] M. Majhi, A. K. Pal, J. Pradhan, S. H. Islam, and M. K. Khan, "Computational intelligence based secure three-party CBIR scheme for medical data for cloud-assisted healthcare applications," Multimedia Tools and Applications, feb 2021.

